Experimental Thermal and Fluid Science 109 (2019) 109870

Contents lists available at ScienceDirect

Experimental Thermal and Fluid Science

journal homepage: www.elsevier.com/locate/etfs

Falling film boiling and pool boiling on plain circular tubes: Influence of surface roughness, surface material and saturation temperature on heat transfer and dryout

Bradley D. Bock[a], Josua P. Meyer[a,*], John R. Thome[b]

[a] Department of Mechanical and Aeronautical Engineering, Faculty of Engineering, the Built Environment and IT, University of Pretoria, Pretoria, South Africa
[b] University of Edinburgh, Edinburgh, United Kingdom

ARTICLE INFO

Keywords:
Boiling
Falling film
Evaporation
Pool boiling
Enhancement factor
Surface
Roughness
Material
Dryout
Plateau
Heat transfer coefficients
R-134a
Thin film boiling
Refrigerant
Organic fluid
Chiller
Spray evaporator

ABSTRACT

Falling film evaporators in the refrigeration industry offer a number of advantages over their flooded counterparts such as improved heat transfer and lower refrigerant charge. Existing literature has not characterised the influence of surface roughness and material on the falling film boiling process. The purpose of this study was therefore to experimentally measure the influence of surface material and roughness on the heat transfer of falling film boiling and pool boiling on the outside of horizontal plain tubes. The falling film enhancement factor and total dryout threshold were also measured in the study. The study was conducted on an experimental set-up at saturation temperatures of 5 °C and 25 °C using refrigerant R-134a at heat fluxes from 20 to 90 kW/m^2 and film Reynolds numbers from 2000 to 0. The outside of plain copper, stainless steel and mild steel tubes were roughened with various grades of sandpaper to achieve roughnesses between 0.1 and 1.9 μm. The tubes were heated by water and as such Wilson plots were conducted to characterize the internal heat transfer. Increases in surface roughness were found to increase both pool boiling and falling film boiling heat transfer coefficients. Changes in surface material decreased the heat transfer coefficients in line with the decrease of the material's thermal effusivity. The falling film enhancement factor was found to increases as surface roughness was increased, but changes in material had no discernible effect. Decreases in saturation temperature decreased pool boiling and falling film boiling heat transfer coefficients and weakly increased the falling film enhancement factor. Changes in surface roughness and material had no discernible influence on total dryout threshold.

1. Introduction

Falling film evaporators in the refrigeration industry that operate in the nucleate boiling regime have great potential due to a number of advantages over their flooded counterparts such as a lower refrigerant charge and improved heat transfer at lower heat fluxes [1]. Lower charge evaporators in particular have safety advantages when poisonous or flammable refrigerants are used. This has become particularly pertinent with the signing of the Kigali amendment to the Montreal protocol which seeks to phase out high global warming potential (GWP) refrigerants [2], with many of the low GWP refrigerants touted to replace the current generation of refrigerants classified as mildly flammable (e.g. hydrofluoro-olefins) or poisonous (e.g. ammonia).

A number of reviews on the topic of falling film boiling in refrigerant evaporators, namely Ribatski and Jacobi [1], Thome [3], Fernandez-Seara and Pardiñas [4] and Abed et al. [5] have shown that much research still needs to be conducted to understand falling film boiling. A significant portion of the research has focussed on enhanced tubes due to their immediate industrial usefulness, while gaps in our fundamental understanding of falling film boiling on plain tubes still remain. Thus this study focusses on falling film boiling on plain tubes in an effort to fill some of these gaps.

A number of falling film boiling studies [6–12] with refrigerants on the outside of plain horizontal tubes have shown that increases in heat flux increased the HTCs up until a point, whereafter the heat transfer coefficients (HTCs) began to decrease. Moeykens et al. [6] and Zhao et al. [10] showed, however, that if the film Reynolds number is increased, the HTCs at lower heat fluxes remained constant while the HTCs at higher heat fluxes increased, which suggests that some form of dryout is the cause for the lowered HTCs at high heat fluxes.

The absolute magnitude of the heat transfer measured on plain copper tubes varies between studies, with the HTCs measured with R-

* Corresponding author.
E-mail address: josua.meyer@up.ac.za (J.P. Meyer).

https://doi.org/10.1016/j.expthermflusci.2019.109870
Received 23 February 2019; Received in revised form 12 June 2019; Accepted 7 July 2019
Available online 08 July 2019

Nomenclature

C	Wilson plot modifier coefficient
c_p	specific heat capacity
D	tube diameter
f	friction coefficient
h	heat transfer coefficient
K	enhancement factor
k	thermal conductivity
L	tube length
$\dot{m}$	mass flow rate
Pr	Prandtl number
P	pressure
q	local heat flux at midpoint of tube length
R_a	mean surface roughness
Re	Reynolds number
Re_f	film Reynolds number
R	thermal resistance
T	temperature
U	overall heat transfer coefficient
$u_c(y)$	combined standard uncertainty of quantity y
x	co-ordinate dimension along the length of the tube

Greek symbols

Γ	mass flow rate of refrigerant on one side of the tube per unit length
μ	dynamic viscosity
ρ	density

Subscripts

c	condensation
dry	dryout threshold
ff	falling film conditions
h	hydraulic
i	internal
l	liquid
o	outer
pb	pool boiling conditions
$probe$	temperature measuring probe
ref	refrigerant
sat	saturated conditions
top	top of tube
w	water
$wall$	tube wall

Superscripts

m	exponent for the relationship between HTC and roughness, $h_o \propto {R_a}^m$

134a of Roques and Thome [7] between 3 and 6 times higher than those measured by Moeykens et al. [6], while the HTCs measured by Zhao et al. [10] fell closer to the data of Moeykens et al. [6]. The arithmetic mean roughness R_a of the plain tubes used by Roques and Thome [7] was 0.8 μm, which is relatively high when compared to the typically quoted roughness range of commercial tubes of 0.2 μm to 0.6 μm [13]. Both Moeykens et al. [6] and Zhao et al. [10] did not state their tube's roughnesses, but this factor may go some way to explaining the differences in the HTC magnitudes.

The film Reynolds number has been shown to influence heat transfer in two distinctive regimes. At low film Reynolds numbers, a significant decrease of HTCs has been shown once the film Reynolds number drops below a threshold, whereafter dryout conditions are experienced with insufficient liquid supplied to maintain a wetted tube [7,10].

A wetted regime occurs above this threshold with the falling film boiling HTCs shown by Jin et al. [11] and Roques and Thome [7] to be relatively insensitive to changes in film Reynolds number with variations less than 5%. Zhao et al. [10], however, found a greater sensitivity of the HTCs to changes in film Reynolds number within the wetted regime, with HTC changing by approximately 10% to 25% within the fully wetted regime. It is difficult to say whether possible differences in tube roughness may have caused these different HTC sensitivities to film Reynolds number or whether other factors, such as differences in the falling film distributors, may be the reason behind this.

The falling film enhancement factor K_{ff}, the ratio of falling film boiling HTC to pool boiling HTC, gives insight into the falling film boiling mechanism. Unfortunately many authors do not explicitly calculate it, such as Moeykens et al. [6], Chien and Chen [9] nor Zhao et al. [10]. Extracting data from their published plots of the falling film boiling and pool boiling HTCs allowed the calculation of their enhancement factors so that it could be compared to those of Roques and Thome [14], who did explicitly calculate it.

This comparison of falling film enhancement factors for plain tubes at saturation temperatures close to 5 °C with R-134a is plotted in Fig. 1. There is significant scatter between the authors. Roques and Thome [14] calculated enhancement factors of 1.4 that were relatively insensitive to variations in heat flux from 20 to 60 kW/m^2.

Both Zhao et al. [10] and Moeykens et al. [6] had enhancement factors that were both lower and more sensitive to changes in heat flux than Roques and Thome [14]. Moeykens et al. [6] conducted their studies at relatively low film Reynolds numbers where some form of dryout can be expected to have deteriorated the heat transfer process, which may account for their lowered results. The reasons for the differences between Zhao et al. [10] and Roques and Thome [14] are difficult to determine. As stated previously, Roques and Thome [14] conducted their tests on tubes with relatively high roughness compared to typical commercial tubes. It can thus be hypothesized that Zhao et al. [10] conducted their tests on smoother tubes, which may have caused the differences in their results. The results of Chien and Chen [9] are difficult to explain.

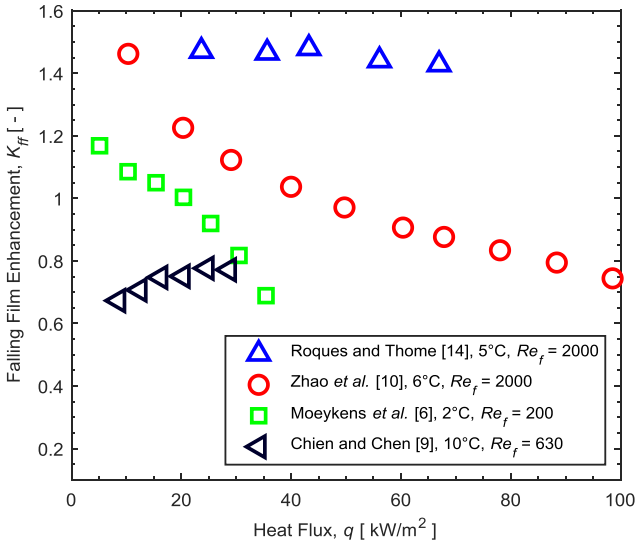

Fig. 1. Comparison of literature values for falling film enhancement factor K_{ff} for plain tubes for R-134a at saturation temperatures close to 5 °C.

Falling film boiling heat transfer has been shown to outperform the respective pool boiling heat transfer not only on the outside of horizontal tubes, but also in thin falling vertical films [15] and in thin stationary horizontal films [16]. Nishikawa et al. [16] in fact found that as the liquid level was dropped in pool boiling experiments of water, ethanol and an aqueous solution of sodium oleate, the HTCs remained relatively constant until the level dropped below approximately 5 mm, whereafter the HTCs increased.

The nature of boiling in thin films, either stationery or moving, is clearly different from pool boiling. Mesler [15] and Cerza and Sernas [17] theorized that the enhancement is caused by bubbles becoming trapped in the thin superheated films, with the increased microlayer evaporation through the bubble base enhancing heat transfer in particular. Mesler and Mailen [18] further hypothesized that the seeding of secondary nucleation sites results from bubbles bursting while being trapped in the thin films.

From literature it thus follows that studies of falling film boiling with refrigerants on plain tubes are fairly limited and there is significant disagreement between results, particularly concerning the falling film enhancement factor. Few authors measure and quote their surface roughness and as such it is difficult to infer the influence of surface roughness on falling film boiling heat transfer and falling film enhancement. Furthermore most studies make use of copper tubes. At present there is thus a research gap as no experimental studies have focussed on quantifying the influence that surface roughness or surface material has on the falling film boiling of refrigerants.

This study aims to experimentally measure the influence of surface roughness and surface material of plain tubes on falling film boiling heat transfer, falling film dryout and the falling film enhancement factor across a range of heat fluxes and at differing saturation temperatures.

2. Experimental setup and test conditions

2.1. Experimental setup

Studies were conducted on a falling film experimental system as illustrated in Fig. 2 which was originally built at the Laboratoire de Transfert de Chaleur et de Masse (LTCM) located at the École Polytechnique Fédérale de Lausanne (EPFL) in Switzerland. The system was previously used for a number of studies under the leadership of Prof JR Thome, such as the falling film condensation work of Gstoehl [19], and falling film boiling work on plain and enhanced tubes of Roques [20], Habert [21] and Christians [22]. The system was reassembled, recommissioned and fully recalibrated in South Africa at the University of Pretoria's Clean Energy Research Group (CERG). What follows is a description of the experimental equipment as was used for this study.

Experiments were conducted within a test chamber (Item 1 in Fig. 2) which consisted of a stainless steel rectangular shell with windows for visual access and removable tube sheets on each end so that tubes could be loaded to create a horizontal tube bank for investigation.

Liquid refrigerant from the bottom of the rig was fed by an oil free gear pump (Item 2) towards the test chamber. The flow rate of the refrigerant was controlled with a variable frequency drive, where a bypass line around the pump was used at low flow rates. The refrigerant subsequently passed through a vibration dampener and Coriolis mass flow meter (Item 3). Thereafter an electric element heater (Item 4) was used for fine tuning of the liquid refrigerant temperature to within 0.5 °C of the saturation temperature on the way to the liquid distributor (Item 5) that spread the refrigerant evenly along the entire length of the tubes. Special care was taken to ensure an even liquid distribution to prevent the refrigerant distribution from influencing the results significantly. Once refrigerant was fed over the tubes, any non-evaporated liquid returned to the bottom of the rig under the action of gravity.

Vapour created by refrigerant boiling on the tubes was driven

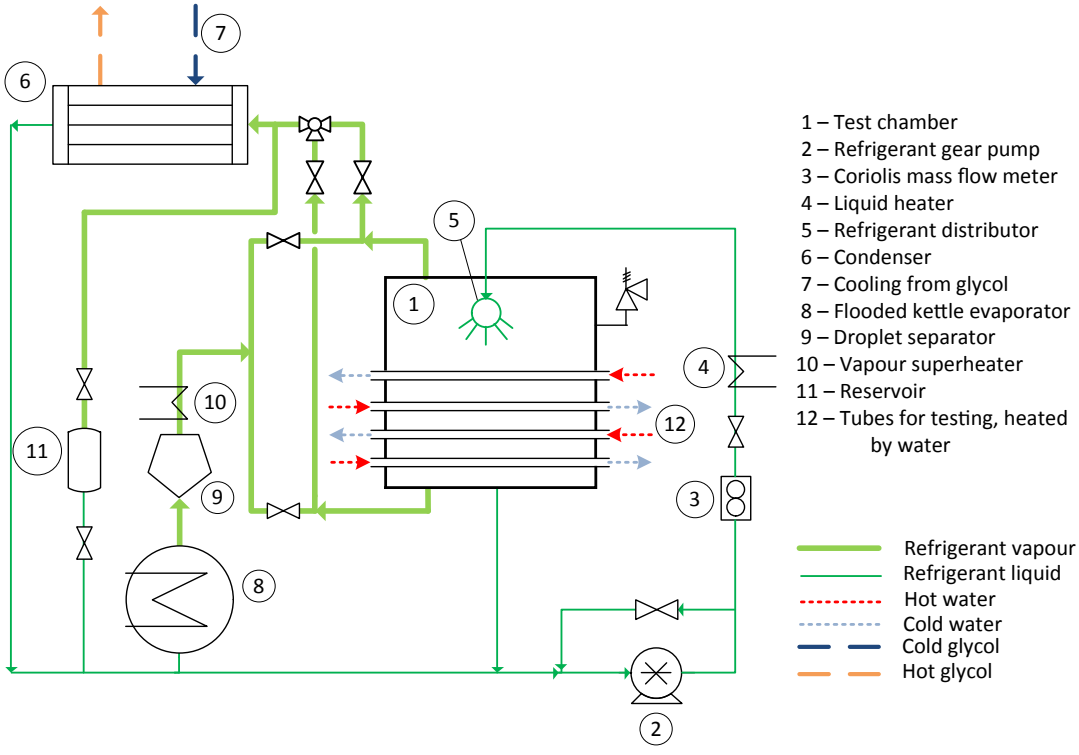

Fig. 2. Schematic of refrigerant loop.

upwards by buoyancy towards an overhead condenser (Item 6), which was cooled by chilled glycol (Item 7) supplied by a separate glycol conditioning loop. The subsequently condensed refrigerant returned by gravity to the bottom section of the rig.

The overall control of the saturation pressure of the refrigerant was achieved with a flooded electric kettle evaporator (Item 8), which served to balance the various heating and cooling loads the test chamber and overhead condenser applied to the refrigerant system. Refrigerant vapour created by the electric evaporator passed through a droplet separator (Item 9) and a fine-tuning electric heater (Item 10) before it reached the test chamber where it could be fed in either from the bottom or the top. For this study vapour was allowed to enter and exit the test chamber from both the top and bottom to ensure no net vapour flow was created. A liquid reservoir (Item 11) together with a float level ensured the electric kettle evaporator did not run dry.

Previous gases were removed from the experimental setup by a vacuum process prior to filling with new refrigerants. A vacuum pump was connected to the system until a pressure of 100 Pa absolute was achieved and maintained. Any non-condensable gases that did remain would collect in the overhead condenser. The success of this process was determined by the difference in saturation temperature calculated from the saturation pressures measured and actual temperatures measured within the test chamber. These were found to differ by no more than 0.2 °C.

The tested tubes were heated with water (Item 12) conditioned by two heat exchangers. The first heat exchanger was supplied with the laboratory's 5 °C utility water and cooled the test chamber water down to a base temperature with the aid of a manual hand valve. The second heat exchanger was supplied with the laboratory's 60 °C utility water. It was heated and controlled to the required set temperature through a computer-controlled valve on the outlet of the hot utility water. This system thus controlled the testing water's temperature as flow rates were changed and compensated for any fluctuations in the utility water temperature. Water was pumped by a multi-stage variable speed drive centrifugal pump through the system. The pump had a bypass line to assist in fine tuning the flow rate.

Table 1
Properties of tubes tested.

Property	Copper tube	Stainless steel	Mild steel	Units
Material grade	C 122	304	A 179	
Outer diameter	19.05*	19.05*	19.05*	mm
Inner diameter	16.65*	16.65*	14.83*	mm
Rockwell hardness B	60 **	92 †	72*	HRB
Thermal conductivity	340 **	16 †	47 ‡	W/mK
Specific heat capacity	0.385 **	0.5 †	0.486 ‡	kJ/kgK
Density	8941 **	8000 †	7850 ‡	kg/m^3
Effusivity	34	8	13	kWs$^{0.5}$/m^{2}K
Notes	Hard drawn seamless	Seamless	Cold drawn seamless	

* Taken from material data sheets.
** (CDA, 2018).
† (AZO, 2001).
‡ (EPRI, 2007).

Pool boiling (Fig. 3a) or falling film (Fig. 3b) experiments were conducted in the test chamber. For pool boiling experiments the test chamber was closed off and filled with refrigerant while for falling film studies liquid refrigerant was evenly distributed along the length of the tube. While the test chamber can accommodate a bank of up to three columns of ten rows of tubes, in this paper only single tubes were tested at a time. The refrigerant used in this study was R-134a.

Pool boiling and falling film studies of the same tubes at the same

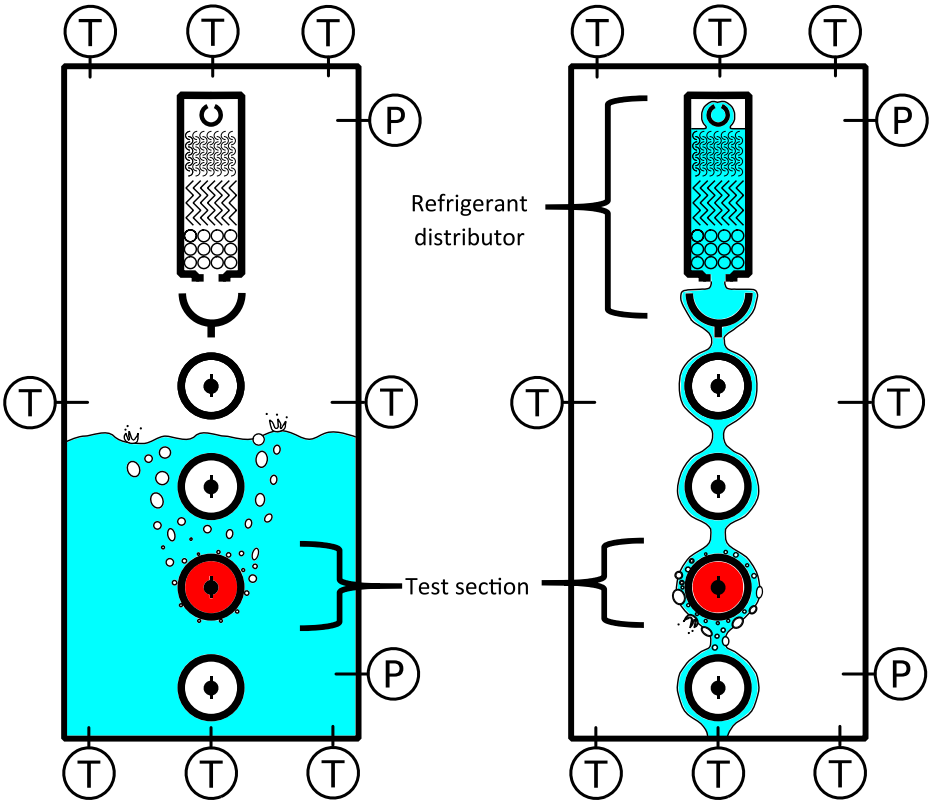

Fig. 3. Schematics of test chamber operation modes and temperature and pressure measuring points.

test conditions were conducted on successive days to minimize differences to further aide reproducibility between the respective data sets and reduce uncertainty in the calculation of the falling film enhancement factor.

2.2. Tube test sections

The properties of the tubes tested for pool and falling film boiling are listed in Table 1. All tubes tested had an outer diameter of 19.05 mm and length of 554 mm. As thermal effusivity is known to be an important wall material influence on pool boiling [13], tubes made from copper, mild steel and stainless steel were tested as they span a relative wide range of effusivities from 8 to 34 $kWs^{0.5}/m^2K$, as detailed in Table 1.

A total of eight tubes (Table 2) were first polished to remove any initial roughness, whereafter they were roughened in a longitudinal direction to varying degrees of roughness. Due to the differences in hardnesses of the tubes, the copper tubes could be roughened with sandpaper (Grits 1200, 600, 100 and 40) by hand. The mild steel and stainless steel tubes could not be roughened by hand and were roughened with an angle grinder fitted with sandpaper discs of grits 1200 and 100.

The tube roughness's were measured with a diamond tip profilometer (Mitutoyo SJ Surftest 210 profilometer) producing results adhering to ISO 4287:1997 and ISO 4288:1998 with a resolution of 0.002 µm. As per ISO 4288:1998, the cut-off length was set to 0.8 mm as the roughness values R_a were lower than 2 µm. The roughness was measured both across and with the grain. Previous papers have not specified the direction of their roughness measurements with regards to the roughness grain [7,23]. To allow for comparison to previous papers it was assumed that previously stated roughnesses were measured against the grain as this is a standard approach when measuring machined surfaces [24]. Thus all roughnesses quoted going forward in this study are those across the grain. Values were cross checked with a diamond tip Alpha-Step 200 profilometer and the average disagreement was less than 0.05 µm.

The roughnesses of the tubes are shown in Table 2 and illustrated in Fig. 4. The grit sandpapers chosen produced increasingly rougher tubes that span and exceed the roughnesses often seen in industrial tubing. Gorenflo and Kenning [13] suggested that a range of 0.2–0.6 µm was typical for commercial tubing, while the roughnesses range from 0.11 to 1.91 µm in this study.

Scanning electron microscopy (SEM) photographs of the surfaces shown in Fig. 5 illustrate that the roughness produced was characterized by long thin channels of relatively uniform nature in the direction of the sandpapering (which was in a longitudinal flow direction).

The tubes were stored for three days after preparation to ensure a stable surface had formed and thereafter tested within three months to minimise the influence of long term surface degradation on the results.

2.3. Instrumentation

The test chamber was instrumented at the top and bottom with two absolute pressure transducers, while the vapour saturation temperature was measured with eight K-type thermocouples along the height and width of the test chamber. The temperature of the refrigerant liquid and vapour that entered and exited the test chamber was also measured. The temperature was monitored so as to ensure saturated conditions and found to be on average within 0.2 °C of the set saturation temperature across the test chamber.

The temperature profile of the hot water inside the test section was measured with a custom developed probe, as illustrated in Fig. 6. The probe consisted of a central 8 mm stainless steel tube with six 0.5 mm K-type thermocouples fed through the tube and protruding out into the water at three evenly spaced locations. At each location there were two thermocouples, one protruding upwards and another downwards. To further ensure the heating water was well mixed within the tube, a wire of rectangular cross section was wrapped around the probe producing a helical mixing spiral.

The mass flow rates of the refrigerant, heating water and cooling glycol were measured with Coriolis mass flow meters.

2.4. Acquisition and control

The data acquisition was performed with a National Instruments (NI) system controlled through LabVIEW software. Each data point captured the average of 30 data points, which themselves were the average of 800 samples recorded at 100 Hz. Thermocouple measurements were fed into a NI TC-2095 terminal chamber, which performed cold junction compensation with the aid of a metallic plate to keep all the junctions at the same temperature and an in-built thermistor to determine the cold junction temperature.

Pressure transducer current outputs were measured and converted into voltage outputs by Sirax TV 808 isolating amplifiers before being fed into the NI TC-2095 terminal chamber. The terminal block was fed into a NI SCXI-1102 thermocouple input module. These modules contained a 2 Hz low pass filter to reduce electromagnetic noise. They were subsequently plugged into a NI SCXI-1000 chassis, which then communicated through a PCI-MIO-16XE-50 acquisition card to a designated measurement PC operating LabVIEW software.

The control of the experimental setup was achieved through a combination of manual valves and switches and automated control valves and heaters via a designated control PC that ran LabVIEW software. The control system data acquisition system was similar to the measurement acquisition system, with the addition of a number of purpose fit modules, such as current measurement with a NI SCXI-1308 terminal block, voltage measurement with a SCXI-1303 terminal block, while outputs were sent with a SCXI-1325 terminal block connected to a SCXI-1124 module.

3. Data reduction

3.1. Film Reynolds number

For the falling film experiments, the mass flow rate of refrigerant on one side of the tube per unit length, Γ_{top}, was defined as the measured mass flow rate of refrigerant fed to the refrigerant distributor on the top of the tube, $\dot{m}_{ref,top}$, per one side of a tube of length L and was thus given by Eq. (1).

$$\Gamma_{top} = \frac{\dot{m}_{ref,top}}{2L} \tag{1}$$

From this the film Reynolds number, Re_f, was defined as

$$Re_f = \frac{4\Gamma_{top}}{\mu_l} \tag{2}$$

Table 2
Tube roughnesses.

Material	Grit	Roughening method	Average mean roughness across roughness grain R_a [µm]	Average mean roughness with roughness grain R_a [µm]
Copper	G1200	Hand	0.12	0.11
	G600	Hand	0.35	0.35
	G100	Hand	0.74	0.47
	G40	Hand	1.37	0.85
Mild steel	G1200	Angle grinder	0.11	0.10
	G100	Angle grinder	1.91	0.70
Stainless steel	G1200	Angle grinder	0.09	0.10
	G100	Angle grinder	1.32	0.81

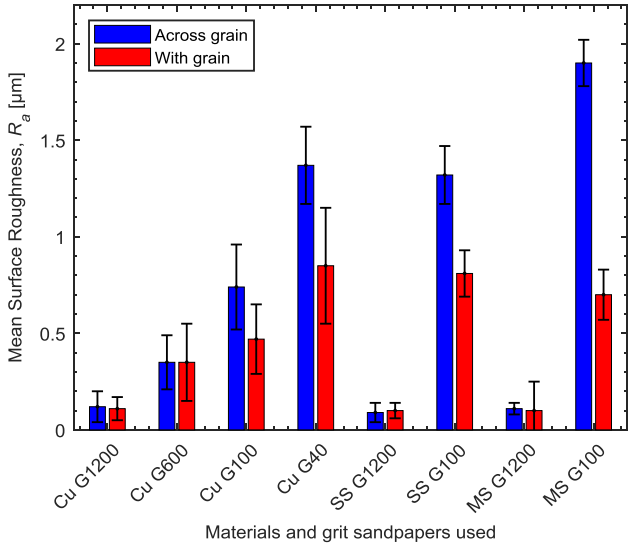

Fig. 4. Mean surface roughnesses across and with the roughness grain of various tubes tested. (Cu = Copper tube; SS = Stainless steel tube; MS = Mild steel tube).

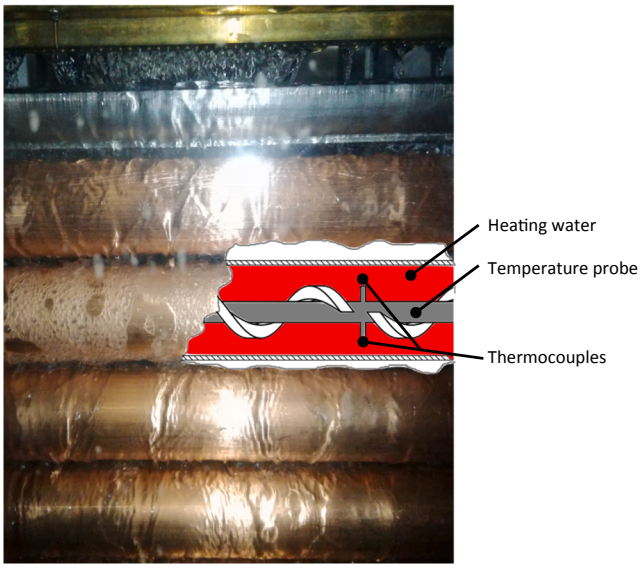

Fig. 6. Photo of test chamber with cut away schematic of test section illustrating measurement probe.

The dynamic viscosity of the liquid refrigerant, μ_l, at the measured temperatures, together with other refrigerant and water thermophysical properties (density, ρ, specific heat, c_p, and thermal conductivity, k) were determined with the aid of REFPROP 8, a software application provided by the National Institute of Standards and Technology [25].

3.2. Local heat flux

In order to determine the local HTC at any point along the length of the instrumented tube, the local heat flux was calculated. As described by Christians [22], the local heat flux was calculated as

$$q = \frac{\dot{m}_w c_p}{\pi D_o}\frac{dT_w}{dx} \tag{3}$$

where $\dot{m}_w$ was the measured water mass flow rate and D_o the measured outside diameter of the tested tube. The temperature gradient, dT_w/dx, was estimated at the midpoint of the tube's length using the gradient of a second order polynomial fit to the measured water temperature profile along the length of the tested tube.

3.3. Internal heat transfer coefficient – Wilson plot

As only the overall HTC of the tube in the test chamber could be measured due to the infeasibility of installing wall temperature sensors on the tube surface, the internal HTC of the test section tube was estimated with the aid of the Wilson Plot method. Initially described by Wilson [26], the methodology employed in this study follows that of Briggs and Young [27] as modified by Van Rooyen et al. [28].

The internal HTC, h_i, was assumed to take the form of the Gnielinski [29] correlation modified by a coefficient C_i which was estimated through a Wilson plot. The internal HTC, h_i, was thus calculated as follows

$$h_i = C_i \frac{(f/8)(Re_w - 1000)Pr_w}{1 + 12.7(f/8)^{0.5}(Pr_w^{2/3} - 1)}\left(\frac{k_w}{D_h}\right) \tag{4}$$

The friction factor, f, was estimated from Petukhov's equation [30] for a smooth tube, based on the Reynolds number of the water flowing through the inside of the tube, Re_w, as follows

$$Re_w = \frac{4\dot{m}_w}{\pi(D_i + D_{probe})\mu_w} \tag{5}$$

where, D_i, was the measured internal diameter of the tested tube and D_{probe} the measured outer diameter of the water temperature probe.

In Eq. (4) the measured hydraulic diameter D_h was given by $D_i - D_{probe}$, while the water Prandlt number Pr_w was calculated as follows

$$Pr_w = \frac{c_{p,w}\mu_w}{k_w} \tag{6}$$

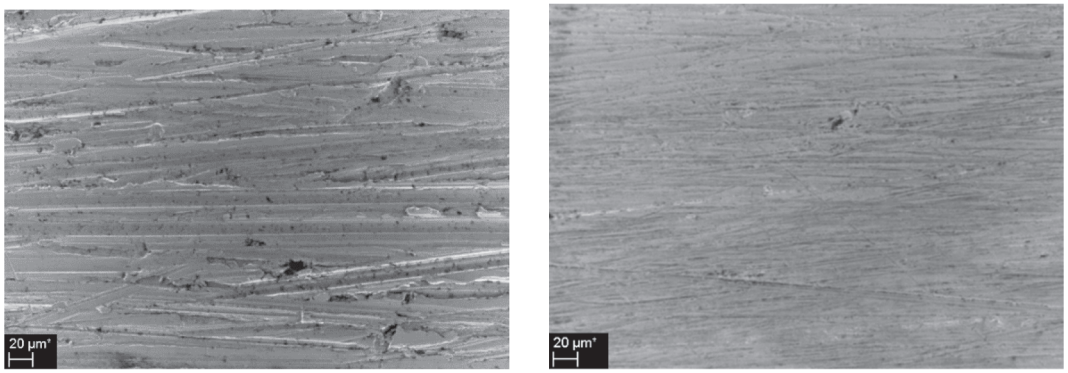

(a) Grit 100 (b) Grit 1200

Fig. 5. Scanning electron microscope (SEM) images of roughened tubes.

3.4. External heat transfer coefficient

The local external HTC, h_o, on the outside of the tube was determined as

$$h_o = \left(\frac{1}{U_o} - R_{wall} - \frac{1}{h_i}\frac{D_o}{D_i}\right)^{-1} \quad (7)$$

The total HTC, U_o, was calculated by

$$U_o = \frac{q}{T_w - T_{sat}} \quad (8)$$

where the water temperature, T_w, was estimated at the midpoint of the tube's length using a second order polynomial fit to the water temperature profile measured along the inside of the tube length and the refrigerant saturation temperature, T_{sat}, was estimated using REFPROP 8 based on the saturation pressure measured at the top of the test chamber.

The wall thermal resistance R_{wall} was determined by

$$R_{wall} = \frac{D_o ln\left(\frac{D_o}{D_i}\right)}{2k_{wall}} \quad (9)$$

3.5. Falling film enhancement factor

The falling film enhancement factor, K_{ff}, was calculated as the ratio of the external falling film HTC $h_{o,ff}$ to the respective external pool boiling HTC $h_{o,pb}$ at the same heat flux and saturation temperature.

$$K_{ff} = \frac{h_{o,ff}}{h_{o,pb}} \quad (10)$$

The pool boiling HTC was interpolated with the aid of a fourth-degree polynomial fit to calculate the HTC at the specific heat flux the falling film HTC was measured.

3.6. Total dryout threshold

The strategies used in previous studies to identify the film Reynolds number at which total dryout occurs were found to be at times not particularly successful and as such a new methodology was employed. In particular many previous strategies made use of the average HTC over the range of film Reynolds numbers tested as a key input into their criterion. These methods often struggled with data from this study where the HTC dropped throughout the film Reynolds number range or where a large amount of data was captured after the film Reynolds number total dryout threshold.

A gradient based approach was decided on in this study, as this would allow for the identification of the point of rapid HTC decrease while ignoring more gradual decreases observed in the data.

The total dryout threshold was defined as the first data point, as the film Reynolds number was increased from 0, which met the following criterion:

$$\frac{dh_o}{dRe_f} < 5 \quad W/m^2K \quad (11)$$

Fig. 7 illustrates the implementation of this strategy on a copper tube with the HTC as a function of film Reynolds number. The gradient, dh_o/dRe_f, is also given in the figure as a function of film Reynolds number. At very low film Reynolds numbers the gradient was very large but as the film Reynolds numbers increased, the gradient became smaller. Applying the dryout criterion, the last data point as the film Reynolds number was increased to have a gradient dh_o/dRe_f below 5 W/m^{2}K occurs at a film Reynolds number of approximately 630 with a corresponding HTC of 15.2 W/m^{2}K.

The new criteria succeeded in a wide variety of experiment conditions to successfully identify the total dryout threshold. The total dryout threshold defined by the method of Christians and Thome [31] is plotted for comparison in Fig. 7. Their method in effect identified the threshold as the first data point that fell below 5% of the mean HTC of the data set. Fig. 7 illustrates that it selected a point that is deep within the dryout regime rather than identifying the threshold point.

3.7. Average deviation

The average deviation between correlations and experimental data was defined as

$$Average\ \ deviation = \frac{1}{n}\sum_{i=1}^{n}\frac{|(Correlation\ \ value) - (Experimental\ \ value)|}{(Experimental\ \ value)} \times 100 \quad (12)$$

in order to facilitate the comparison of experimental data to correlations. The correlation values were calculated at each of the experimental data points.

4. Uncertainties

The expanded standard uncertainties of the various sensors were determined as per the methodology employed in Dunn [32]. The precision was assumed to be equal to the uncertainty of the reference probes used and the bias was assumed to be equal to the standard deviation of the noise the probes measure. The probes were calibrated with linear regression calibration fits. The law of propagation of uncertainty as detailed in JCGM 100:2008 [33] was applied to these fits to capture the influence of the fits on the bias and precision. The resulting expanded standard uncertainties of the probes are listed in Table 3, with a 95% confidence interval employed.

The uncertainty of the roughness measurements was estimated through a Type A evaluation and an assumed normal distribution of roughnesses about the mean value measured (as detailed in JCGM 100:2008 [33]) with a confidence interval of 95% employed. The individual roughness uncertainties are illustrated in Fig. 4 with the overall average roughness uncertainty found to be 0.17 μm as listed in Table 3. Fig. 4 illustrates that the absolute magnitude of the roughness uncertainties increases as the roughness increases and that the differences in roughness between samples of a particular material are significant when compared to the uncertainties, suggesting a sufficiently spread sample of roughnesses has been chosen.

The combined standard uncertainties of the various calculated

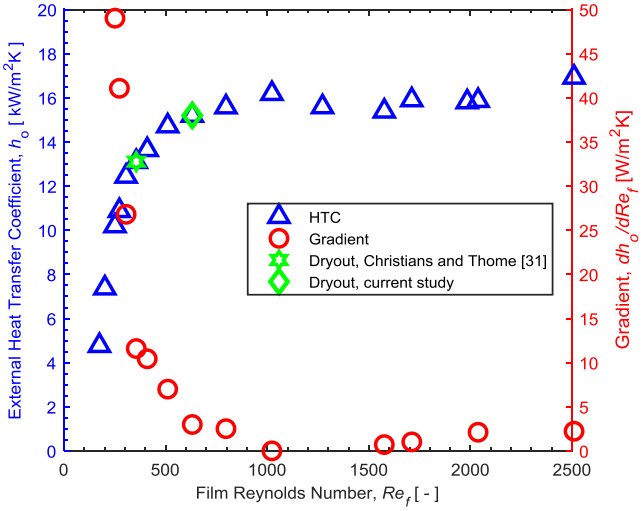

Fig. 7. Falling Film boiling HTC on a copper tube with a surface roughness of 0.74 μm as a function of film Reynolds number Re_f at 25 °C at a heat flux of 50 kW/m^2 illustrating the dryout point selection method as per Christians and Thome [31]and the current study.

Table 3
Average uncertainties of measurements and calculated quantities.

Quantity		Symbol	Uncertainty
Probes	Temperature	$u_c(T)$	0.1 K
	Pressure	$u_c(P)$	0.2%
	Water mass flow rate	$u_c(\dot{m}_w)$	0.2%
	Surface roughness	$u_c(R_a)$	0.17 μm
Output	Heat flux	$u_c(q)$	9.0%
	Heat transfer coefficient	$u_c(h_o)$	33%
	Falling film enhancement	$u_c(K_{ff})$	5.2%

quantities were determined through the law of propagation of uncertainty. Equations were determined to calculate the uncertainties of these quantities based on the uncertainties of the probe measurements. The derivation of these equations was documented in detail by Christians [22] and the resulting calculated uncertainties are listed in Table 3. The uncertainties of the thermo-physical properties calculated with the aid of REFPROP 8 software [25] are listed in Christians [22].

The calculation of the uncertainty of the falling film enhancement factor K_{ff} in this study however differs from Christians [22]. Considering that K_{ff} is the ratio $h_{o,ff}/h_{o,pb}$, which are measurements of the same quantity under different conditions, the two input quantities are thus dependant. The subsequently derived uncertainty equation for K_{ff} was

$$u_c^2(K_{ff}) = {K_{ff}}^2\left(\frac{u_c(h_{o,ff})}{h_{o,pb}}\right)^2 (K_{ff}-1)^2 \tag{13}$$

The resulting average uncertainties as function of heat flux across the range of tests are shown in Table 3. These uncertainties are illustrated in Fig. 8 as function of heat flux for a typical case. The average HTC uncertainty was 33% (it varied between a minimum of 25% at a heat flux of 90 kW/m^2 and a maximum of 45% at a heat flux of 20 kW/m^2). These uncertainties are comparable to previous researchers who worked on this same piece of equipment [7,31] and other similar experimental set-ups [10]. Measurements at heat fluxes lower than 20 kW/m^2 were not practical and were avoided due to the continued rise in the uncertainty of the HTC as the heat flux lowered. However, the average falling film enhancement uncertainty was significantly lower at 5.2% as it was calculated from two dependant properties. It varies from 8.7% at a heat flux of 20 kW/m^2 to 0.2% at a heat flux of 90 kW/m^2.

5. Validation

The Wilson plots conducted acted as an initial validation stage, as the internal heat transfer modifying coefficient C_i (Eq. (4)) determined in this paper of 1.25 compared satisfactorily to previous researchers who worked with plain tubes on this same experimental setup with values of 1.27 [20], 1.18 [21] and 1.29 [34].

Condensation tests were used to validate the measurement system of the experimental apparatus as the literature for pool boiling and falling film studies often exhibit a wide spread of results as well as a lack of surface roughness information. Furthermore the most successful modelling solutions for boiling are semi-empirical as the production of correlations for nucleate boiling is fraught with difficulty [35], which makes them unsuitable for stand-alone validation purposes.

Condensation tests were chosen specifically as the Nusselt solution for condensation on tubes without inundation [3] is a solution that has been shown by previous work to agree well with experimental data, with previous results lying within 5% of the solution [36]. Thus the Nusselt solution could serve as a reference for comparison and validation. The results for a single horizontal plain copper tube with condensation on the outside of the tube at a saturation temperature of 30 °C with a surface roughness, R_a, of 0.15 μm and no inundation are given in Fig. 9 as a function of the condensation temperature difference ΔT_c.

The experimental data compares well with the Nusselt solution, as 93% of the data falls within 5% of the Nusselt solution. The average deviation between the data and the Nusselt solution was 2.3%.

Pool boiling tests conducted on a single plain copper tube of roughness R_a of 0.74 μm at a saturation temperature of 5 °C with R-134a are presented in Fig. 10. The HTCs are compared to the results of Roques and Thome [7] who conducted tests under identical conditions with a similar roughness R_a of 0.8 μm as well as the correlations of Cooper [37] and Gorenflo and Kenning [13]. The results matched closely to those of Roques and Thome [7] at the upper end of the heat flux range of 80 kW/m^2. However, the two datasets diverged at the lower end of the heat flux range, with a difference of 40% at a heat flux of 20 kW/m^2. Given that the uncertainty of the data increases towards 45% as heat fluxes lower towards 20 kW/m^2, this deviation is expected.

The Cooper [37] and Gorenflo and Kenning [13] correlations compared well with the results. The average deviation between the data and Cooper correlation was 9.6%, with 95% of the data falling within 15% of the correlation. The average deviation between the data and Gorenflo and Kenning's correlation was 9.2%, with 95% of the data falling within 16% of the correlation.

Falling film boiling tests were compared to the study by Roques and Thome [7], with data collected on copper tubes at a saturation temperature of 5 °C with R-134a and compared in Fig. 11. Similar to the pool boiling data comparison, the data is more closely matched at higher heat fluxes, with a difference of approximately 20% at a heat flux of 60 kW/m^2, while the data diverges to a difference of approximately 70% at the lower heat flux of 20 kW/m^2. A possible reason for the differences between the datasets, despite being measured on the same equipment, could be the various improvements in calibration and roughness measurements that have occurred since the study by Roques and Thome [7], as well as the higher uncertainties at lower heat fluxes.

The average deviation between the data and the Ribatski and Thome [38] correlation was 34% with 48% lying within 30% of the correlation. The Ribatski and Thome correlation has close agreement with the Roques and Thome [7] data, which can be expected as it incorporated data from Roques and Thome [7] into its fitting process. Other falling film correlations were not considered as they do not take surface roughness into account.

The short term repeatability of the experiment is illustrated in Fig. 11 with three successive readings taken at each set point, with the data points differing by less than 3% of each other. The longer term repeatability of the experiments is also illustrated in Fig. 11, with two

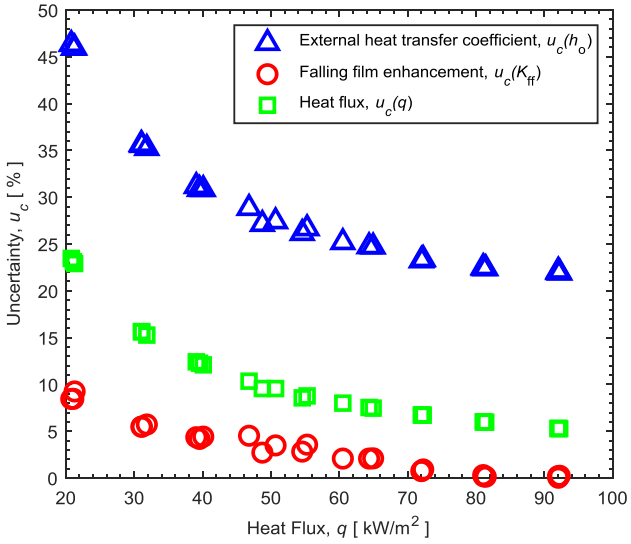

Fig. 8. Uncertainties as a function of heat flux at 5 °C for a copper tube under falling film boiling conditions with a R_a of 0.12 μm.

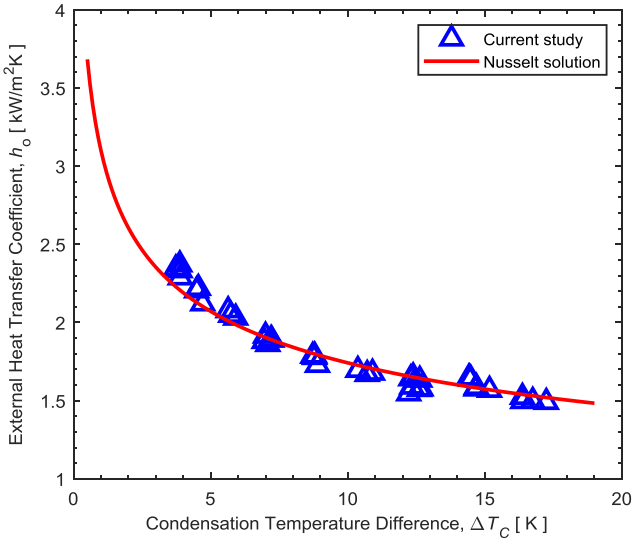

Fig. 9. Condensation for a single tube with no inundation at a saturation temperature of 30 °C.

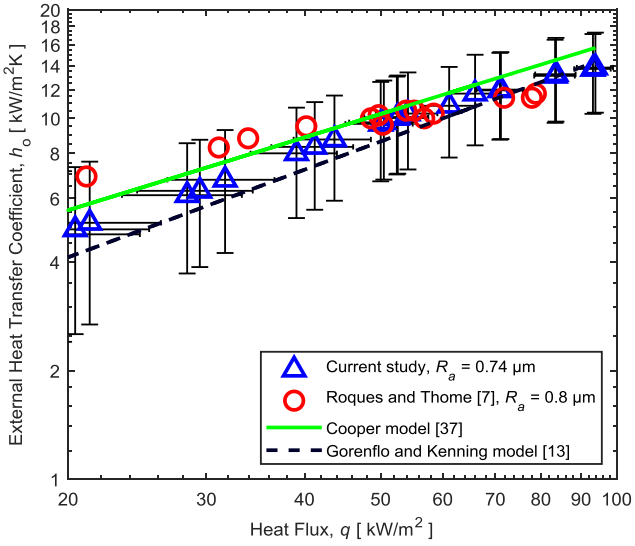

Fig. 10. Pool boiling of copper tubes at a saturation temperature of 5 °C.

nearly identical studies conducted five months apart having produced data that highly overlapped, with an average deviation of 5.4% between the repeated data and a curve fit through the original data.

6. Pool boiling results

Pool boiling results were first recorded on the tubes so as to provide a comparative reference to the falling film results and thus allow the calculation of the falling film enhancement factors (Section 7). The results presented here thus serve as the baseline to compare the falling film results to. As a secondary objective, given the scarcity of data of pool boiling of refrigerants on mild steel and stainless steel tubes, these results aide in further understanding pool boiling mechanisms under these conditions.

6.1. Influence of roughness and saturation temperature on heat transfer

The HTC measured under pool boiling conditions for a range of different roughness copper tubes as a function of heat flux is shown in Fig. 12 for saturation temperatures of 5 °C and 25 °C. Errors bars were omitted on this figure and all subsequent figures to ensure data clarity.

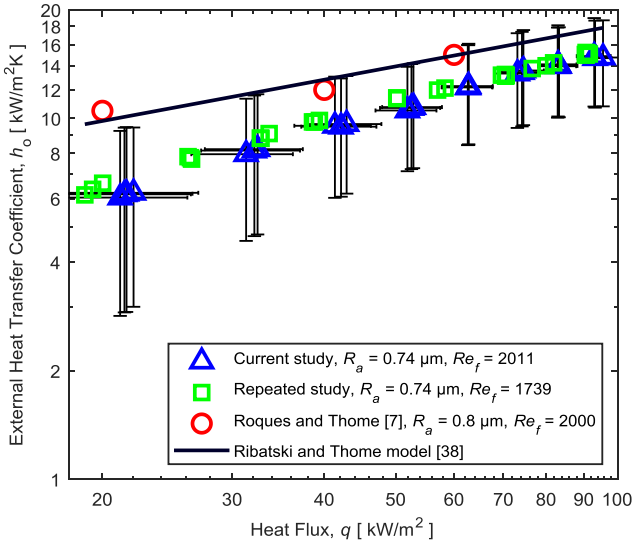

Fig. 11. Falling film boiling on a copper tube at a saturation temperature of 5 °C.

The HTCs for all the tubes increased "linearly" on the double log plot as the heat flux was increased. The increases in roughness R_a resulted in an increase in HTC due to an increase in active nucleation sites, as is well documented in previous studies [13,35].

The influence of the roughness on the HTC was characterised by the fit of the relation $h_o \propto R_a{}^m$ to the experimental data, with the results for the copper tubes under pool and falling film boiling conditions listed in Table 4. The pool boiling results were found to approximately adhere to Stephan's relation of $h_o \propto R_a{}^{0.133}$ [39] for copper tubes in refrigerant.

The increase in saturation temperature from 5 °C to 25 °C increased the HTC by approximately 50% to 30% across the range of heat fluxes for all roughnesses. The increase is to be expected given the well-known influence of pressure on boiling heat transfer [13,35]. While surface roughness has been shown to have a stronger effect at lower pressures [40], this effect could not be distinguished in this study.

6.2. Influence of surface material on heat transfer

The HTC's as a function of heat flux of three different material tubes with relatively smoother finishes at saturation temperatures of 5 °C and 25 °C under pool boiling conditions are presented in Fig. 13. In general the HTC's increased linearly on the double log plot as the heat flux was increased. However, the HTCs of the mild steel tube were shown to be less sensitive to increases in heat flux than the copper and stainless steel tubes.

The copper tube is shown to have the highest HTC, followed by the mild steel tube and then the stainless steel tube. This follows the trend of the thermal effusivity of the tubes, which is considered an influential property of surface materials on the heat transfer process in pool boiling [13].

The increase in saturation temperature again shows an increase in HTCs as the temperature is raised across all three materials. Copper and stainless steel increased by between 54% and 18% and 35% to 29% respectively with the increase in saturation temperature. Mild steel was shown to be less sensitive to the saturation temperature increase, increasing by between 32 and 10% across the heat flux range.

The HTCs of rougher different material tubes as a function of heat flux are shown in Fig. 14. The trends displayed are similar in form to that of the smoother tubes illustrated in Fig. 13. The mild steel is shown to be less sensitive to the increase in roughness than copper and stainless steel, despite having the highest roughness of the three tubes tested in Fig. 14.

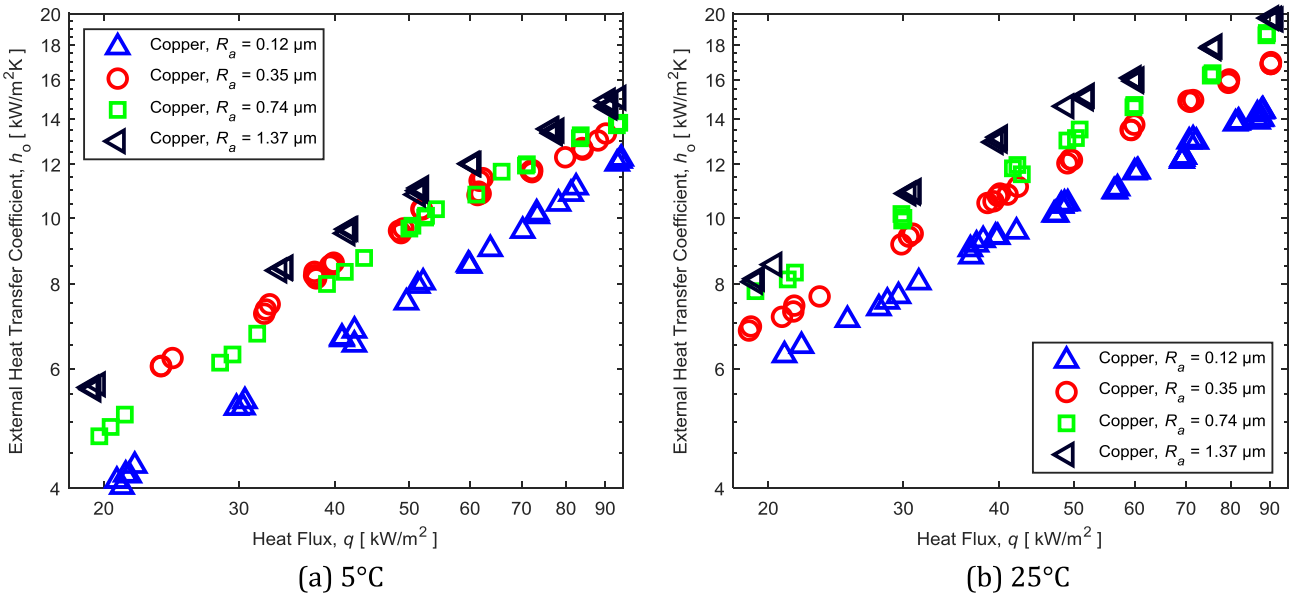

Fig. 12. Pool boiling with different roughnesses of copper tube at different saturation temperatures.

Table 4
Relationship between external HTC and surface roughness for copper tubes.

Boiling mode	Saturation temperature [°C]	Dependence of external HTC on surface roughness
Pool boiling	5	$h_o \propto R_a^{0.110}$
Pool boiling	25	$h_o \propto R_a^{0.125}$
Falling film	5	$h_o \propto R_a^{0.167}$
Falling film	25	$h_o \propto R_a^{0.206}$

7. Falling film results

7.1. Influence of roughness and saturation temperature on heat transfer

The HTCs as a function of heat flux for falling film boiling conditions are shown in Fig. 15. A range of different roughness copper tubes were tested at saturation temperatures of 5 °C and 25 °C with a film Reynolds number of approximately 2100.

The falling film HTCs are shown to mostly exhibit similar overall trends to the comparative pool boiling results in Fig. 12 with the HTCs displaying a similar sensitivity to increases in heat flux. However as higher heat fluxes are reached, the falling film HTCs begin to tail off and become less sensitive to increases in heat flux. This is due to partial dryout resulting in a drop-off of heat transfer, despite the high film Reynolds number.

The falling film HTCs however increased more as roughness was increased when compared to the respective pool boiling results. At 20 kW/m^2 when the roughness R_a was increased from 0.12 μm to 1.37 μm, the falling film HTCs increased by 75% compared to an increase of only 50% for the comparable pool boiling HTCs. The influence of the roughness on the HTCs for the falling film studies for copper tubes is shown in Table 4 and was found to adhere to the relationship $h_o \propto R_a^{0.167}$ at 5 °C and $h_o \propto R_a^{0.206}$ at 25 °C. These exponents are larger than the equivalent for pool boiling as listed in Table 4 and further illustrate that falling film boiling is more sensitive to increases in roughness than pool boiling.

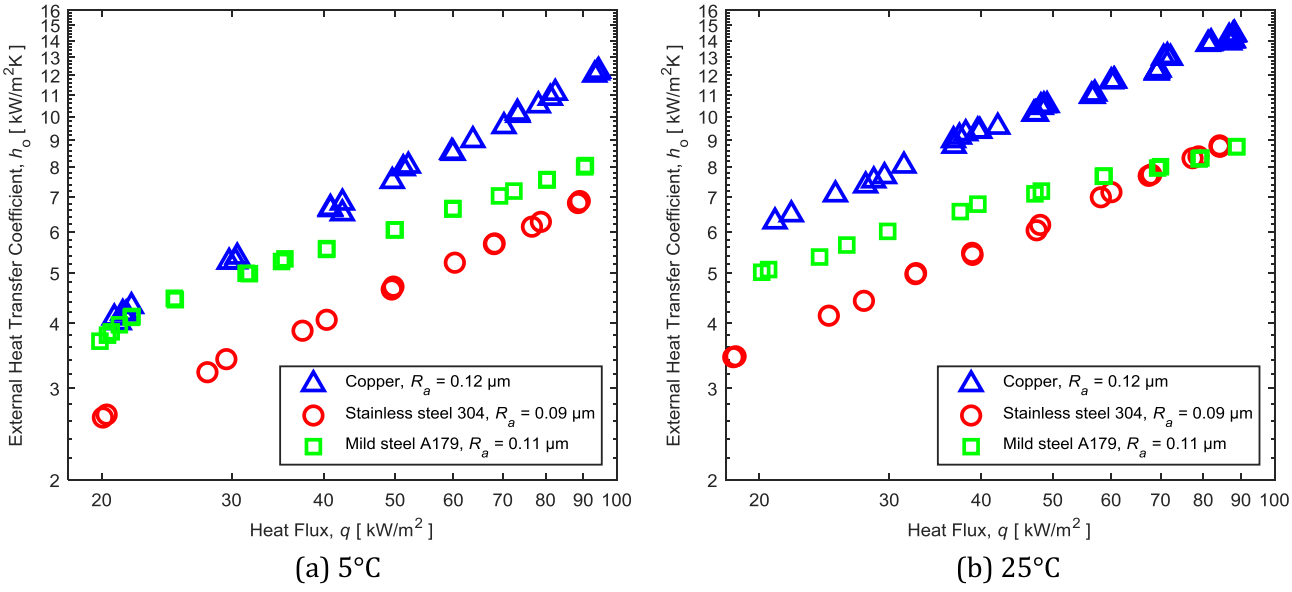

Fig. 13. Pool boiling with smoother tubes of different materials at different saturation temperatures.

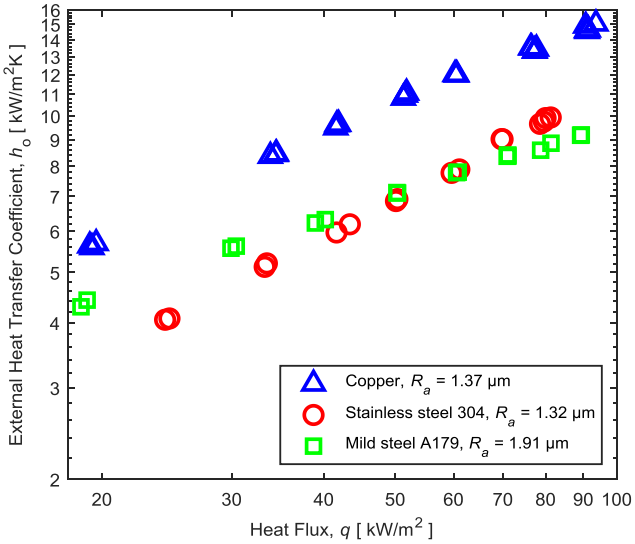

Fig. 14. Pool boiling at 5 °C with different material rougher tubes.

The differing impacts of roughness on the two modes of boiling is further illustrated by the falling film enhancement factor, K_{ff}, shown as a function of heat flux for the range of different roughness copper tubes in Fig. 16 for saturation temperatures of 5 °C and 25 °C with a film Reynolds number of approximately 2100. Falling film boiling mostly outperformed pool boiling, with enhancement factors varying from 1 to 1.3. As discussed in Section 2, this can be attributed to the enhancement mechanisms that have been suggested to be influential in the thin film boiling process, namely the roles of increased microlayer evaporation [15,17] and the secondary nucleation mechanism [18,41].

The enhancement was weakly influenced by heat flux, with the enhancement decreasing by approximately 10% as the heat flux increases from 20 to 90 kW/m^2 at 5 °C, while at 25 °C the enhancement factor was insensitive to changes in heat flux across the range tested.

The falling film enhancements generally increased as the roughness of the tubes was increased for copper tubes, with the enhancement factor ranging from 1 to 1.3 as the surface roughness was increased from 0.12 μm to 1.37 μm. The reason that rougher tubes benefit more from falling film conditions than their smoother counterparts is likely due to the greater bubble density on rougher tubes due to their greater nucleation site density. This greater bubble density would result in an increased enhancement of heat transfer compared to pool boiling due to increased microlayer evaporation and increased secondary nucleation mechanisms. A visualisation study with a high speed camera is recommended to further investigate this hypothesis.

The falling film enhancement factor appears weakly dependant on the saturation temperature, with the enhancement factors increasing by between 0 and 15% as the saturation temperature was dropped from 25 °C to 5 °C. Considering the theorized importance of the bubbles in falling film enhancement, two possible causes of this phenomena have been identified. Firstly the increased surface tension as a result of the lower saturation temperature may lead to longer bubble life as the bubbles are swept within the falling film. Secondly the bubble sizes are expected to be larger at the lower saturation temperature due to the associated lower saturation pressure [42]. Either of these two factors could result in greater microlayer evaporation as the bubbles are swept along in the falling film compared to higher saturation temperatures. Considering the relatively weak influence of saturation temperature seen in this study, further investigation with experimental equipment that can be tested across a greater saturation temperature range is recommended for future research.

The trends regarding falling film heat transfer performance are noted to be less clear at 5 °C than 25 °C, most likely through experimental uncertainty. However when comparing the results of the smoothest and roughest tubes to each other, the trends discussed are clearly applicable.

7.2. Influence of surface material on heat transfer

The falling film HTCs as a function of heat flux for different materials of smoother tubes are shown in Fig. 17 at saturation temperatures of 5 °C and 25 °C, while the HTCs as a function of heat flux are shown for rougher tubes at a saturation temperature of 5 °C in Fig. 18. Both tests were operated with film Reynolds numbers of approximately 2000.

The general trends again follow those of the comparable pool boiling results, with the HTCs increasing as the heat flux is increased, with mild steel being less sensitive to the increases in heat flux than copper or stainless steel. Again the magnitude of the HTCs follows the trend of the thermal effusivities, with copper outperforming mild steel

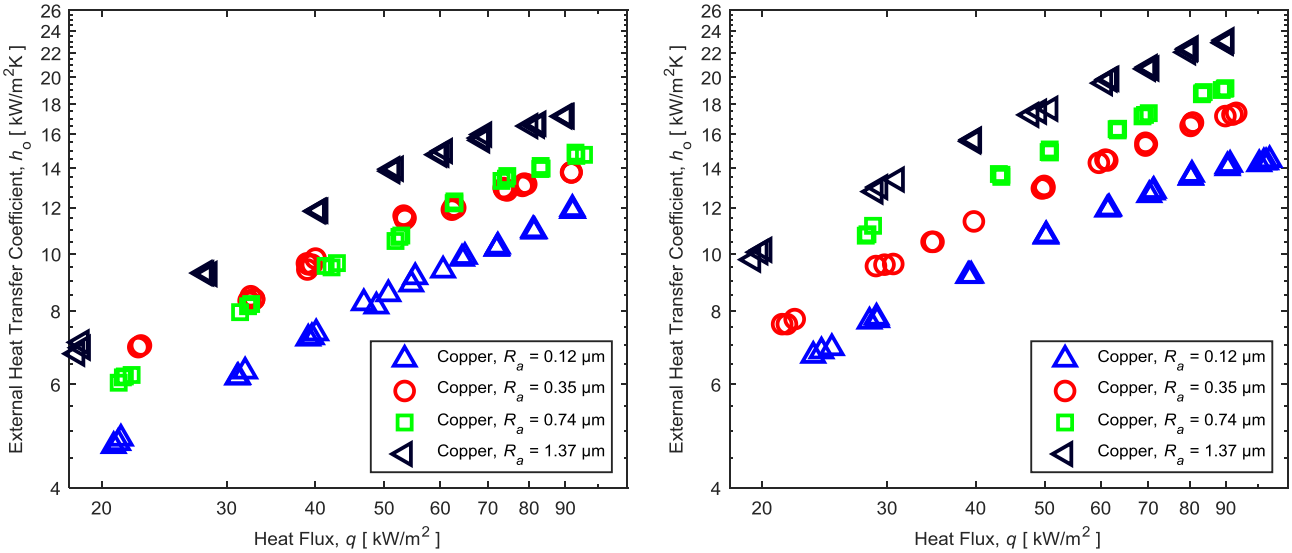

Fig. 15. Falling film boiling HTC's as function of heat flux with different roughnesses of copper tube at a film Reynolds number of approximately 2100 at different saturation temperatures.

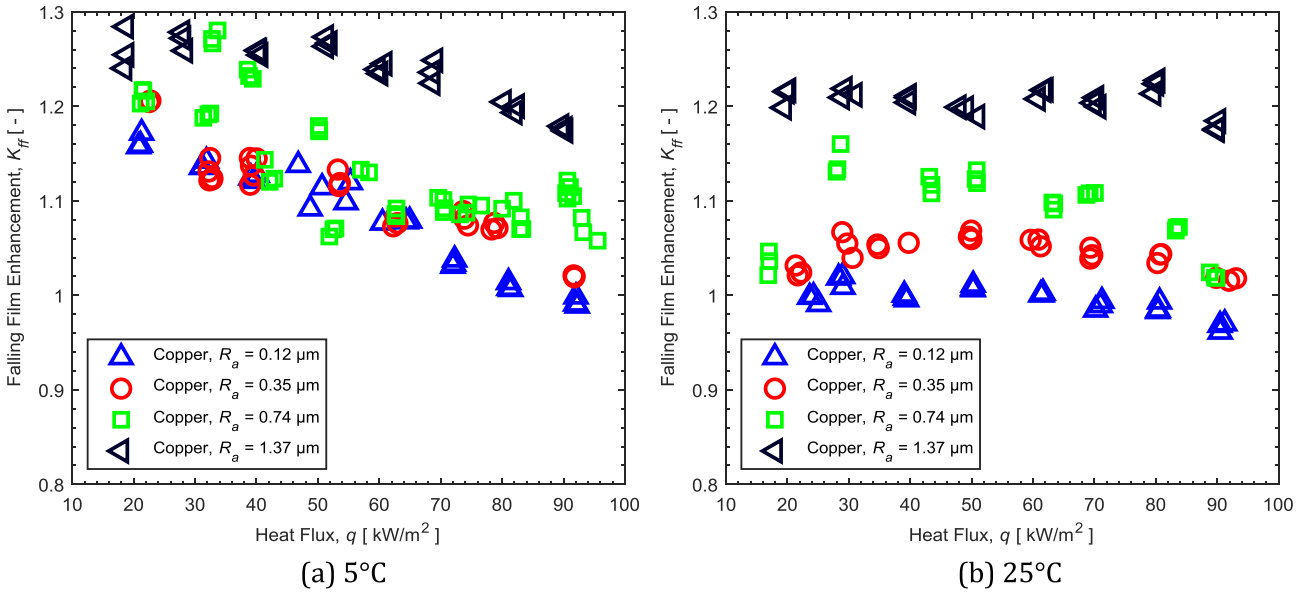

Fig. 16. Falling film enhancement, K_{ff} , with different roughnesses of copper tube at a film Reynolds number of approximately 2100 at different saturation temperatures.

which outperforms stainless steel. At lower heat fluxes the mild steel has comparable heat transfer to the copper tubes, but as the heat flux increases its lower heat flux sensitivity means that it has comparable heat transfer performance to stainless steel at higher heat fluxes.

The falling film enhancement factor K_{ff} as a function of heat flux for smoother and rougher tubes of different material at a saturation temperature of 5 °C and film Reynolds number of approximately 2000 are shown in Fig. 19a. The enhancement factors were weakly sensitive to the heat flux, with the enhancement factors decreasing by less than 10% as the heat flux was increased from 20 to 90 kW/m^2. All three materials tested showed an increase in enhancement factor as the roughness was increased.

The falling film enhancements as a function of heat flux at a saturation temperature of 25 °C of the smoother different material tubes are shown in Fig. 19b. There was very little falling film enhancement under these conditions, with all materials exhibiting enhancement factors close to one. The factors were also relatively insensitive to changes in heat flux.

The difference in tube materials did not significantly influence the falling film enhancement factors, with both the smoother and rougher tube enhancement factors within 10% of each other. It follows that the wall material did not significantly influence the various mechanisms suggested that cause the falling film enhancement. This suggests that while the wall material influences the overall boiling process through the conduction of heat to the nucleation sites, it does not influence the falling film enhancement mechanisms.

Compared to the comparable enhancement factors at a saturation temperature of 5 °C, the enhancement factors decreased slightly for all materials at 25 °C. Considering that this was observed for all three materials, this suggests that the reduction in falling film enhancement as saturation temperature was reduced was not dependant on the wall material and rather influenced only by the fluid's properties, possibly the reduced surface tension at higher saturation temperatures or increased bubble size at lower pressures, as already discussed.

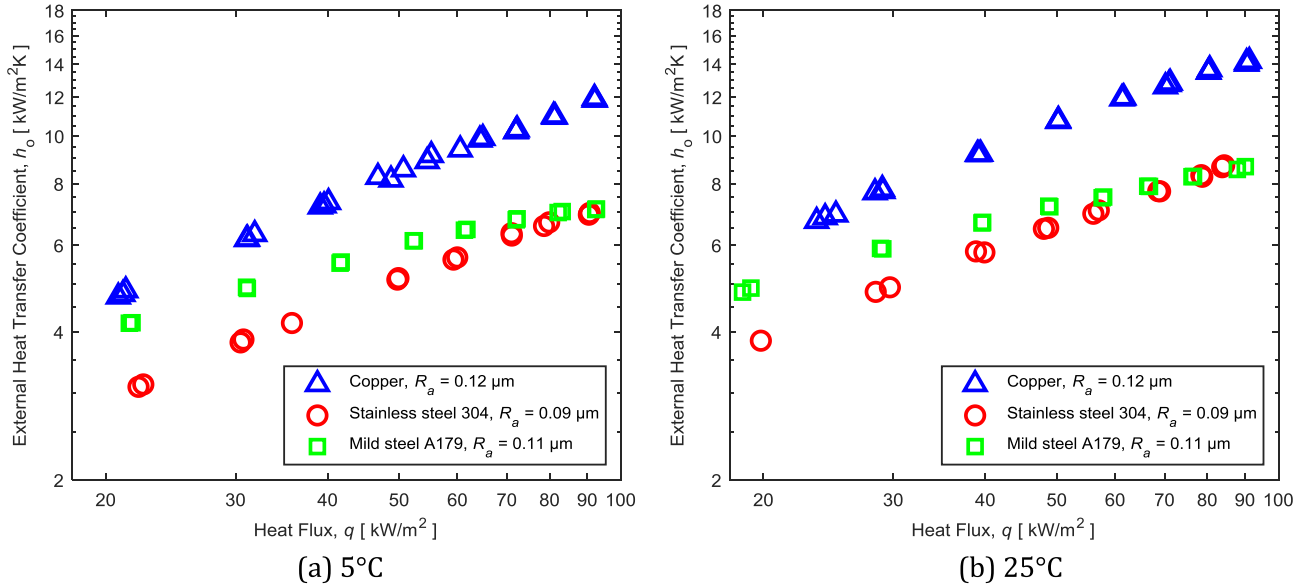

Fig. 17. Falling film boiling with different material smoother tubes at a film Reynolds number of approximately 2000 at different saturation temperatures.

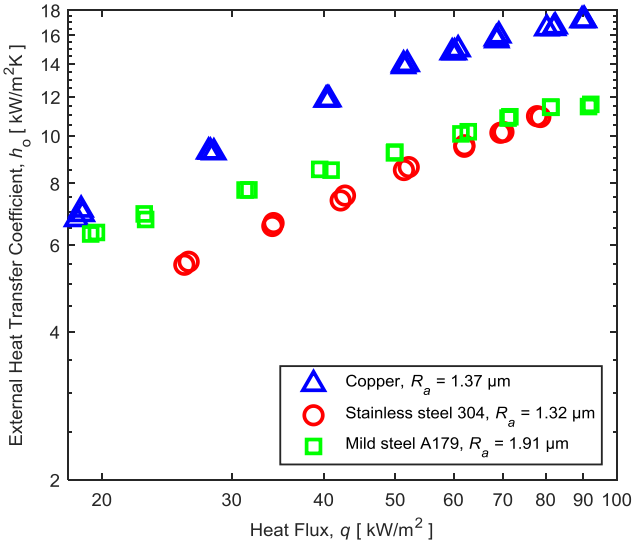

Fig. 18. Falling film boiling at a saturation temperature of 5 °C as function of heat flux with different material rougher tubes at a film Reynolds number of approximately 2000.

8. Dryout results

8.1. Influence of film Reynolds number on heat transfer

A typical plot of the HTC's as a function of film Reynolds number is shown in Fig. 20. The results are for plain copper tubes of roughness R_a of 0.17 μm (Fig. 20a) and 0.74 μm (Fig. 20b) which were tested at a saturation temperature of 5 °C and at three heat fluxes. Both tubes at all three heat fluxes followed similar general trends of relatively stable HTCs as the film Reynolds number was decreased from a maximum until a rapid drop off in heat transfer occurs, caused by total dryout of the tubes.

The cause of the rapid decrease in HTC resulting in total dryout is relatively well understood, with the falling film breaking down and dry patches appearing on the tube at the low film Reynolds number conditions. This was visually confirmed during both this study and previous studies [43].

The rougher tube at all heat fluxes and the smoother tube at 20 kW/m^2 exhibit a region where the HTC is practically insensitive to film Reynolds number changes, often referred to as the plateau region. The HTC is seen to change less than 5% for these tubes for film Reynolds numbers above 500. Roques and Thome [7] and Ribatski and Thome [38] observed similar behaviour when they performed similar experiments on a plain tubes of roughness R_a of 0.8 μm with R-134a at a 5 °C saturation temperature up to heat fluxes of 55 kW/m^2. Jin et al. [11] found a similar plateau region when testing with R134a, R290 and R600a with plain tubes of unspecified roughness.

However, the smoother tube at higher heat fluxes of 50 and 80 kW/m^2 exhibits a plateau region with greater sensitivity to changes in film Reynolds number. The HTC drops by approximately 15% as the film Reynolds number is dropped from 2000 to 500. A falling film study by Zhao et al. [10] with R-134a at saturation temperatures of 6 °C, 10 °C and 16 °C on plain copper tubes also exhibited a plateau region with higher sensitivity to changes in film Reynolds number.

A similar difference in plateau region sensitivity can be seen when Jin et al. [11] compared their heat transfer results for falling film boiling of plain tubes at 6 °C to those of Zhao et al. [10] who tested under near identical conditions with the same experimental set-up. Jin et al. found their falling film plateau region to be very insensitive to changes in film Reynolds number, while the data of Zhao et al. [10] showed a greater plateau region sensitivity. Jin et al. [11] did not offer a possible explanation for the differences and noted that they were within experimental uncertainty limits. The surface roughness of the tubes was not recorded by either Jin et al. [11] or Zhao et al. [10].

A possible cause may be imperfections in the fluid distribution along the length of the tube. Despite every effort made in this study to ensure even fluid distribution along the length of the tubes, it was also noted through visual observation that even at high film Reynolds numbers (above 2000) dry patches would occasionally form and then immediately disappear on both smooth and rougher tubes.

Thus there may have been maldistribution of the fluid for the smoother tubes that led to localised areas along the length of the tube experiencing temporary instances of partial dryout, even at high film Reynolds numbers. This phenomena would worsen as the film Reynold's number decreased, thus causing a reduction in HTC.

A possible physical explanations is that as the smoother tubes operate at higher wall superheats due to lower HTCs. The relatively hotter surface may promote dryout more readily through rapid evaporation of localised thin areas compared to the colder surface of the rougher tubes.

Further detailed visualisation studies to better understand this

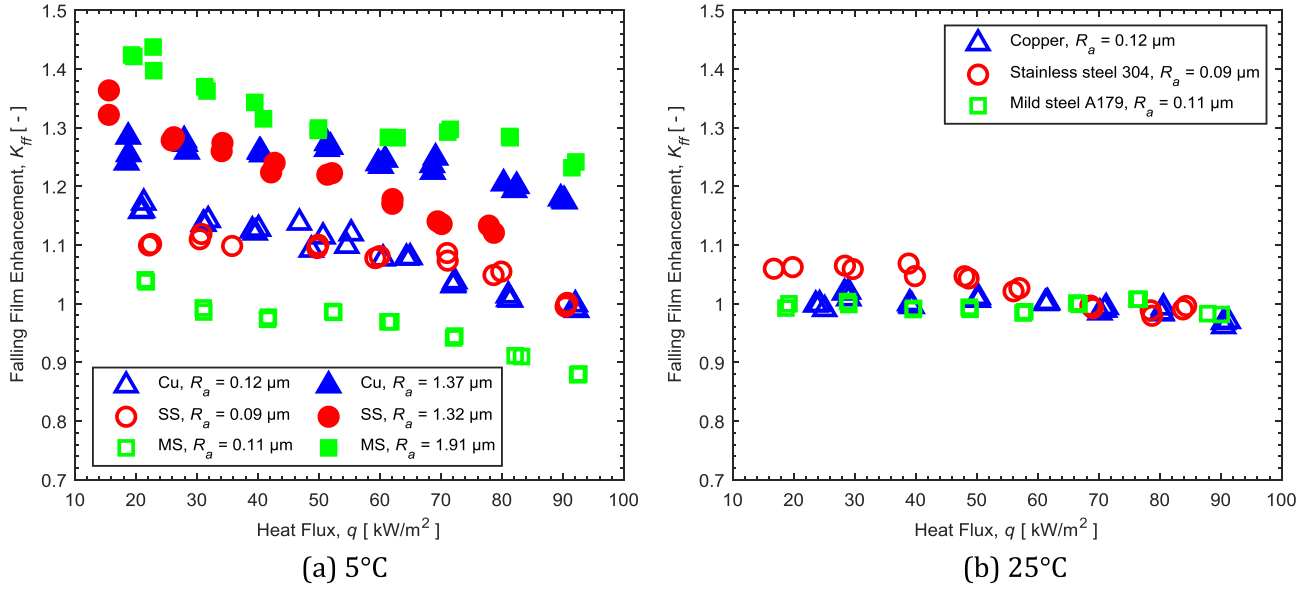

Fig. 19. Falling film enhancement K_{ff} as function of heat flux with different material smoother tubes at a film Reynolds number of approximately 2100.

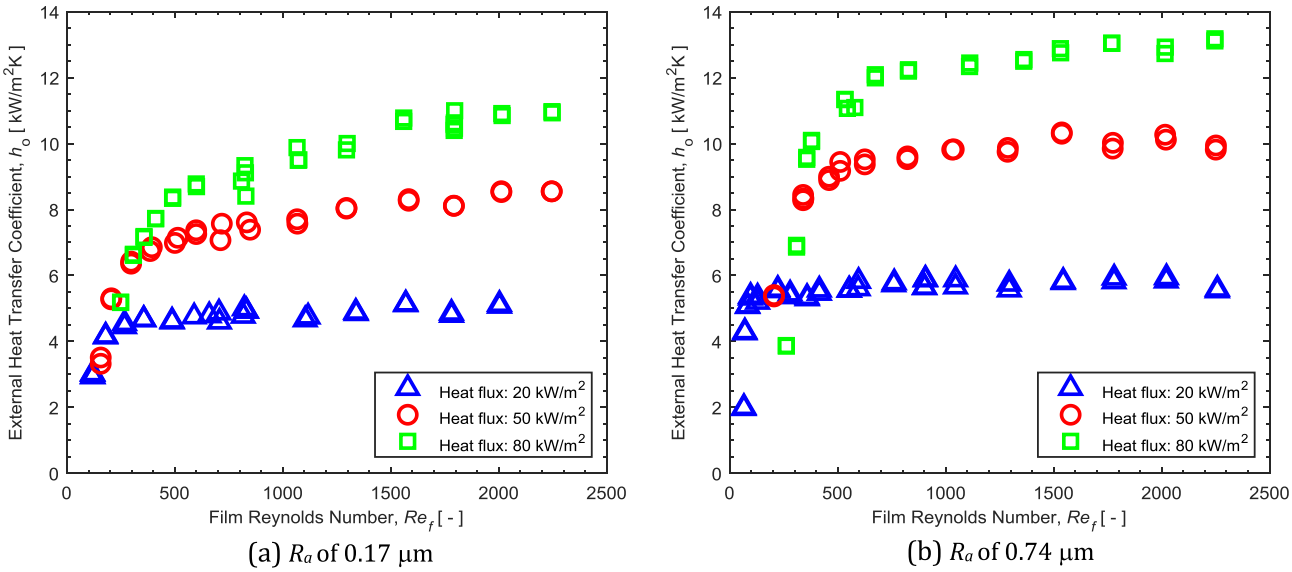

Fig. 20. Falling film boiling HTC as a function of the film Reynolds number at a saturation temperature of 5 °C on plain copper tubes.

phenomenon are recommended to determine whether this sensitivity is indeed some form of dryout phenomenon as hypothesised here or rather caused by another physical process.

8.2. Influence of surface roughness and saturation temperature on total dryout threshold

The threshold film Reynolds number at which total dryout occurs, $Re_{f,dry}$, as a function of heat flux is illustrated in Fig. 21 for copper tubes tested at saturation temperatures of 5 °C and 25 °C and roughnesses R_a of 0.12 μm and 0.74 μm. Also plotted is the evaporative limit, which is the minimum film Reynolds number that can support the corresponding heat flux, assuming all heat is transferred from the tube to the refrigerant and the refrigerant evaporates as a result.

The general trend is that the total dryout threshold increased as the heat flux increased and followed the trends cited by numerous other authors [7,10,31]. The increase in total dryout threshold approximately followed that of the increase in the evaporative limit, except for the rougher copper tube (R_a = 0.74 μm) at the saturation temperature of 25 °C.

Changes in roughness and saturation temperature were not shown to have a discernible influence on the total dryout threshold in this study. Given the inherent difficulty in determining the total dryout threshold and the relative coarseness of the methods used, influences of a smaller magnitude may not be detectable with the methods used in this study. Larger saturation temperature or roughness ranges than used in this study may also be needed to elicit if any influence is present.

8.3. Influence of surface material on total dryout threshold

The total dryout threshold as a function of heat flux for different material tubes at a saturation temperature of 5 °C is shown in Fig. 22. The total dryout threshold shows a similar trend across all three materials, with the total dryout threshold increasing as heat flux is increased proportionally to the increase in the evaporative limit. The wall material did not show to have a strong influence on the total dryout threshold in this study.

9. Conclusions

The purpose of this study was to experimentally measure the influence of surface roughness and surface material of plain tubes on the falling film boiling heat transfer, dryout and enhancement factors. Studies were conducted on plain tubes of varying roughness and material across a range of heat fluxes and film Reynolds numbers at two saturation temperatures. High speed falling film boiling visualisation are recommended as a future avenue of research to provide greater insight into the phenomena seen here.

The conclusions that were drawn are as follows:

(1) The falling film enhancement factor increased as surface roughness increased for all material tubes tested, with the enhancement factor ranging from 1 to 1.4 as the roughness ranged from 0.09 μm to 1.91 μm. It is hypothesized that the greater bubble density of rougher tubes increases the enhancement mechanisms proposed, such as greater microlayer evaporation of the sliding bubbles within the falling film. The respective pool boiling and falling film HTCs increased as surface roughness was increased.
(2) The surface material was found to have no discernible influence on falling film enhancement, but did influence the pool boiling and falling film HTCs, with HTCs increasing as the material effusivity and thermal conductivity of the tubes was increased.
(3) The falling film enhancement was found to be weakly influenced by

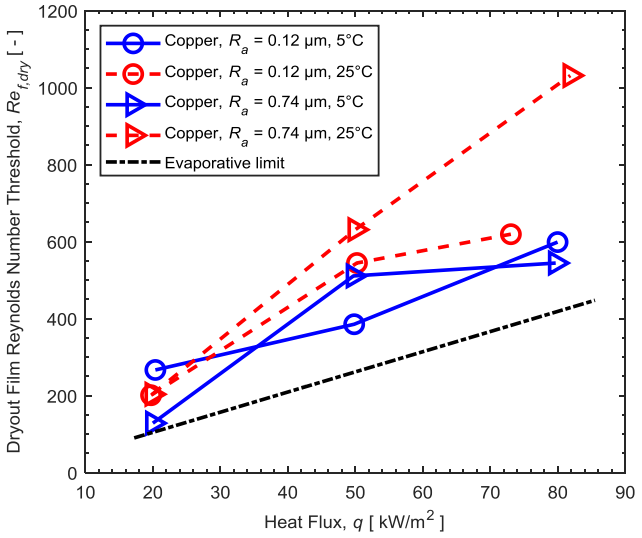

Fig. 21. Total dryout threshold $Re_{f,dry}$ as a function of heat flux for different roughness copper tubes.

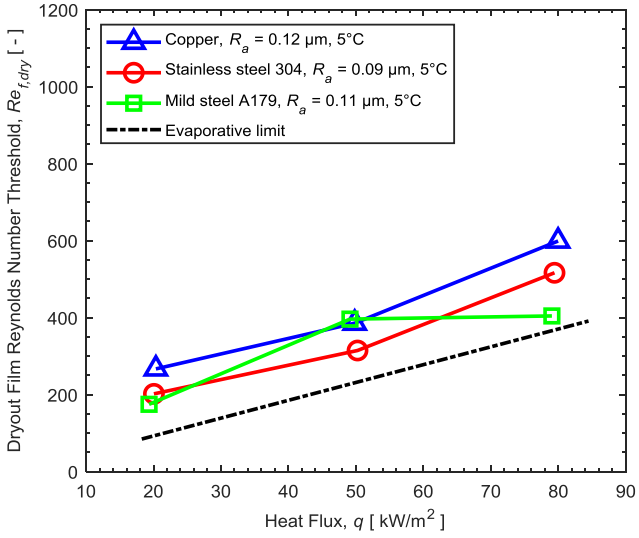

Fig. 22. Total dryout threshold $Re_{f,dry}$ as a function of heat flux for different material tubes at a saturation temperature of 5 °C.

changes in saturation temperature, with the enhancement increasing as saturation temperature decreased by between 0 and 15%. The saturation temperature also influenced the respective pool boiling and falling film HTCs, increasing them as the saturation temperature was increased. Further studies at larger saturation temperature differences are recommended for further investigation.

(4) A plateau region was found where the HTCs of the fully wetted tubes were fairly insensitive to changes in film Reynolds numbers. This insensitivity did vary across the tubes, with the HTCs of rougher tubes changing by approximately 5% as film Reynolds numbers varied from 500 to 2000, while the HTCs of smoother tubes varied by approximately 15%. Once the film Reynolds number dropped below a threshold, all tubes tested exhibited a significant drop in HTCs due to total dryout.

(5) The total dryout threshold was shown to increase as heat flux was increased. The total dryout threshold was not shown to be significantly influenced by surface roughness, surface material or saturation temperature.

Declaration of Competing Interest

It is hereby confirmed that the authors have no conflicts of interest.

Acknowledgement

This project has received funding from the European Union's Horizon 2020 research and innovation programme under the Marie Skłodowska-Curie grant agreement No. 778104.

References

[1] G. Ribatski, A.M. Jacobi, Falling-film evaporation on horizontal tubes – a critical review, Int. J. Refrig. 28 (2005) 635–653.
[2] UNEP, Amendment to the montreal protocol on substances that deplete the ozone layer, United Nations Environmental Program, Art IV (1) (2016).
[3] J.R. Thome, Engineering Data Book 3, Wolverine Tube Inc, 2004.
[4] J. Fernandez-Seara, Á.Á. Pardiñas, Refrigerant falling film evaporation review: description, fluid dynamics and heat transfer, Appl. Therm. Eng. 64 (2014) 155–171.
[5] A.M. Abed, M.A. Alghoul, M.H. Yazdi, A.N. Al-Shamani, K. Sopian, The role of enhancement techniques on heat and mass transfer characteristics of shell and tube spray evaporator: a detailed review, Appl. Therm. Eng. 75 (2015) 923–940.
[6] S.A. Moeykens, W.W. Huebsch, M.B. Pate, Heat transfer of R134a in single-tube spray evaporation including lubricant effects and enhanced surface results, in, American Society of Heating, Refrigerating and Air-Conditioning Engineers, Inc., Atlanta, GA (United States), 1995.
[7] J.F. Roques, J.R. Thome, Falling films on arrays of horizontal tubes with R134a, part 1: boiling heat transfer results for four types of tubes, Heat Transfer Eng. 28 (2007) 398–414.
[8] L.-H. Chien, Y.-L. Tsai, An experimental study of pool boiling and falling film vaporization on horizontal tubes in R245fa, Appl. Therm. Eng. 31 (2011) 4044–4054.
[9] L.H. Chien, R.H. Chen, An experimental study of falling film evaporation on horizontal tubes using R-134a, J. Mech. 28 (2012) 319–327.
[10] C.-Y. Zhao, W.-T. Ji, P.-H. Jin, W.-Q. Tao, Heat transfer correlation of the falling film evaporation on a single horizontal smooth tube, Appl. Therm. Eng. 103 (2016) 177–186.
[11] P.-H. Jin, Z. Zhang, I. Mostafa, C.-Y. Zhao, W.-T. Ji, W.-Q. Tao, Heat transfer correlations of refrigerant falling film evaporation on a single horizontal smooth tube, Int. J. Heat Mass Transf. 133 (2019) 96–106.
[12] D. Jige, H. Miyata, N. Inoue, Falling film evaporation of R1234ze(E) and R245fa on a horizontal smooth tube, Exp. Therm Fluid Sci. 105 (2019) 58–66.
[13] D. Gorenflo, D.B.R. Kenning, Pool boiling (chapter H2), VDI Heat Atlas, Springer-Verlag, Berlin, Heidelberg, 2010, pp. 757–792.
[14] J.F. Roques, J.R. Thome, Falling films on arrays of horizontal tubes with R134a, part 2: flow visualization, onset of dryout, and heat transfer predictions, Heat Transfer Eng. 28 (2007) 415–434.
[15] R. Mesler, A mechanism supported by extensive experimental evidence to explain high heat fluxes observed during nucleate boiling, AIChE J. 22 (1976) 246–252.
[16] K. Nishikawa, H. Kusuda, K. Yamasaki, K. Tanaka, Nucleate boiling at low liquid levels, Bull. JSME 10 (1967) 328–338.
[17] M. Cerza, V. Sernas, A bubble growth model for nucleate boiling in thin, falling, superheated, laminar, water films, Int. J. Heat Mass Transf. 28 (1985) 1307–1316.
[18] R. Mesler, G. Mailen, Nucleate boiling in thin liquid films, AIChE J. 23 (1977) 954–957.
[19] D. Gstoehl, Heat transfer and flow visualization of falling film condensation on tube arrays with plain and enhanced surfaces, Ph.D. thesis École Polytechnique Fédérale de Lausanne, Lausanne, Switzerland, 2004.
[20] J.-F. Roques, Falling film evaporation on a single tube and on a tube bundle, Ph.D. thesis École Polytechnique Fédérale de Lausanne, Lausanne, Switzerland, 2004.
[21] M. Habert, Falling film evaporation on a tube bundle with plain and enhanced tubes, Ph.D. thesis École Polytechnique Fédérale de Lausanne, Lausanne, Switzerland, 2009.
[22] M. Christians, Heat transfer and visualization of falling film evaporation on a tube bundle, Ph.D. thesis École Polytechnique Fédérale de Lausanne, Lausanne, Switzerland, 2010.
[23] J.M.S. Jabardo, G. Ribatski, E. Stelute, Roughness and surface material effects on nucleate boiling heat transfer from cylindrical surfaces to refrigerants R134a and R123, Exp. Therm Fluid Sci. 33 (2009) 579–590.
[24] Mitutoyo, Quick guide to surface roughness measurement, in, Mitutoyo America Corporation, 2016.
[25] E.W. Lemmon, M.L. Huber, M.O. McLinden, NIST reference fluid thermodynamic and transport properties—REFPROP, NIST Standard Reference Database 23 (2002) v7.
[26] E.E. Wilson, A basis for rational design of heat transfer apparatus, Trans. ASME 37 (1915) 47–82.
[27] D.E. Briggs, E.H. Young, Modified wilson plot techniques for obtaining heat transfer correlations for shell and tube heat exchangers, Chemical Engineering Progress Symposium Series, AIChE, New York, NY, 1969, pp. 35–45.
[28] E. Van Rooyen, M. Christians, J.R. Thome, Modified Wilson plots for enhanced heat transfer experiments: current status and future perspectives, Heat Transfer Eng. 33 (2012) 342–355.
[29] V. Gnielinski, New equations for heat and mass-transfer in turbulent pipe and channel flow, Int. Chem. Eng. 16 (1976) 359–368.
[30] B.S. Petukhov, Heat transfer and friction in turbulent pipe flow with variable physical properties, in: J.P. Hartnett, T.F. Irvine (Eds.), Advances in Heat Transfer, Elsevier, 1970, pp. 503–564.
[31] M. Christians, J.R. Thome, Falling film evaporation on enhanced tubes, part 1: experimental results for pool boiling, onset-of-dryout and falling film evaporation, Int. J. Refrig. 35 (2012) 300–312.
[32] P.F. Dunn, Measurement and data analysis for engineering and science, 2nd ed., CRC Press, 2010.
[33] JCGM 100: 2008, Evaluation of Measurement Data—Guide for the Expression of Uncertainty in Measurement, 2008.
[34] F. Agostini, Boiling on a tube bundle: heat transfer, pressure drop and flow patterns, Ph.D. thesis École Polytechnique Fédérale de Lausanne, 2008.
[35] W.M. Rohsenow, J.P. Hartnett, Y.I. Cho, Handbook of heat transfer, McGraw-Hill, New York, 1998.
[36] D. Gstoehl, J.R. Thome, Film condensation of R134a on tube arrays with plain and enhanced surfaces: Part 1— experimental heat transfer coefficients, J. Heat Transfer 128 (2006) 21–32.
[37] M. Cooper, Saturation nucleate pool boiling—a simple correlation, Inst. Chem. Eng. Symp. Ser (1984) 785–793.
[38] G. Ribatski, J.R. Thome, Experimental study on the onset of local dryout in an evaporating falling film on horizontal plain tubes, Exp. Therm. Fluid Sci. 31 (2007) 483–493.
[39] K. Stephan, Beitrag zur Thermodynamik des Wärmeüberganges beim Sieden, Ph.D. thesis Verlag nicht ermittelbar, 1963.
[40] G. Ribatski, J.M.S. Jabardo, Experimental study of nucleate boiling of halocarbon refrigerants on cylindrical surfaces, Int. J. Heat Mass Transf. 46 (2003) 4439–4451.
[41] R. Mesler, Research on nucleate boiling, Chem. Eng. Educ. 16 (1982) 152–156.
[42] R.B. Mesler, J.T. Banchero, Effect of superatmospheric pressures on nucleate boiling of organic liquids, AIChE J. 4 (1958) 102–113.
[43] G. Ribatski, J.R. Thome, A visual study of R134a falling film evaporation on enhanced and plain tubes, 5th International Symposium on Multiphase Flow, Heat Mass Transfer and Energy Conversion, Xi'an, China, (2005).